 doi:10.20944/preprints202209.0382.v1

*Article*

# Effect of Temperature in Zno and Related Computational Studies

**R. Dash[1] and A.S. Bhattacharyya [1,2] ***

[1]Department of Nano Science and Technology
[2]Centre of Excellence in Green and Efficient Energy Technology (CoE GEET), Central University of Jharkhand, Brambe, Ranchi: 835205
* Correspondence: 2006asb@gmail.com; arnab.bhattacharya@cuj.ac.in

**Abstract:** ZnO was synthesized by Sol gel method using zinc nitrate as precursor at different calcination temperatures. Nucleation of ZnO crystallites and their growth with rise in temperature was observed. Exciton bands and lattice imperfections affected the absorption spectra. The decrease in band gap with temperature was due to the formation of defect energy levels. Phonon assisted non-radiative transitions caused broadening of the peaks. The possibility of tuning the band gap of ZnO by changing the temperature was explored. Simulation studies showed transition to single phase with rise in temperature.

**Keywords:** ZnO; sol gel; temperature; band gap; simulation

## 1. Introduction

Zinc Oxide (ZnO) has properties of high refractive index, high binding energy, high thermal conductivity, good biocompatibility, antibacterial and UV protection. It has numerous applications like in electronic devices, photocatalysis, gas sensing, bio medical, skin treatment, filter in cigarettes and biometric membrane **[1, 2].**

ZnO is an n-type semiconductor with band gap 3.3 – 3.4 eV and exciton binding energy of 60 meV, transparent in the visible region and a less toxic material. ZnO has been blended with other transition metal oxides, polymers, reduced graphene oxide (rGO) and other materials for enhanced electrochemical properties. ZnO–NiO@rGO NiO–ZnO-modified g-$C_3N_4$ **[3, 4]**, ZnO / rGO, Zr-doped ZnO; SnOx-ZnO **[5-14]**, ZnO-$Co_3O_4$; ZnO/CoO **[15, 16]**, ZnO/Polymer Nanocomposites **[17, 18]** and ZnO/NiO, $Al_2O_3$-ZnO, ZnO nanorod@Ni–Co **[19-21]** are few examples.

Its electrical properties can be improved by doping with trivalent metal ions. The parent $Zn^{+2}$ ion being divalent, the trivalent dopant (eg: $Al^{+3}$) provides an extra electron which results in enhanced electrical conductivity. Al-ZnO materials have been reported to give high optical

 doi:10.20944/preprints202209.0382.v1



transmittance apart from high carrier density making it highly applicable for transparent electrodes in solar cells **[22]**.

ZnO has preferential cytotoxicity against cancer cells which kills cancerous cells without affecting normal cells. This ability can be improved by metal ion doping. The wide band gap property of ZnO nanoparticles helps in induction of intracellular reactive oxygen species which actually leads to photoactive oxidative damage of biomolecules, killing the cancer cells. This photo activity can be achieved by creation of large number of conduction electrons and holes which usually takes place on exposure to UV radiation. However, creation of more defects by metal ion doping can also create sufficient charge carriers and omit the requirement of UV light **[23, 24].**

The direct gap semiconductor materials like GaAs, CdTe, GaN, ZnO etc have either a zinc-blend or a wurtzite crystal lattice. In zinc-blend semiconductors, the valence band splits into three sub-bands referred to as the heavy-hole, light-hole and spin-off bands. In the wurtzite semiconductors, the valence band splits into three non-degenerated subbands referred to as A, B, and C bands.

ZnO nanoparticles have been prepared by various physical and chemical methods. During chemical synthesis, changing the chemical nature of the constituents and temperature alters the shape of the nanoparticles formed from spherical to wire like or plate like etc **[22]**. In this work we have synthesized ZnO by Sol gel method and analyzed the effect of temperature

## 2. Experimental

Zinc oxide nanoparticles were synthesized through sol-gel method using zinc nitrate as a precursor. 5.9513 g of zinc nitrate with 40 ml of water is prepared and added with 1.0048 g of urea. The sample was kept for stirring for 3 hr with a temperature of 120$^{o}$C. As a result ZnO is formed and was transferred to petty dish. Calcination was done in an oven for 10 hr at 100$^{o}$C temperature. The formed sample weighed 1.4097 g The characterizations were done using XRD (Proto A-XRD), UV-Vis spectrometer (UV 3600 Plus, Shimadzu, Japan and Photoluminescence spectrometer (Fluromax-4, Horiba Scientific, USA). The simulation studies were carried out in MATLAB using octave online free software **[25]**.

 doi:10.20944/preprints202209.0382.v1



## 3. RESULTS AND DISCUSSIONS

The XRD patterns of samples prepared and dried at three different temperatures are given in **Fig 1 (a)** along with the patterns obtained by so-gel and green synthesis **(Fig 1b)**. A phase change is observed to be occurring with change in temperature. The peaks obtained at 200$^{o}$C matched with the XRD peaks of ZnO given in the literature. The crystal structure is wurtzite. Crystallite size using Scherer's formula $D = \frac{k\,\lambda}{\beta\,Cos\theta}$ after deconvolution of the peaks showed 18 nm crystallite formations at 200$^{o}$C for the most intense peak at 36$^{O}$ corresponding to (1 0 1) plane. The sample was however in amorphous state even at 100 $^{o}$C and the crystals had just started to nucleate which was evident from the fact that crystallite size obtained was of the order of Å (**Fig 2 & 3**). This is basically grain growth through diffusion where larger grains grow at the expense of smaller ones and the driving force being the difference in strain energy. Increased temperature causes higher diffusion leading to faster grain growth.

The results were compared with the ones synthesized by Sol gel process using zinc acetate dihydrate, absolute alcohol and $H_2O_2$ to prepare ZnO. A green synthesis of ZnO was also done by taking 10ml of Hawaiian hibiscus leaves extract. XRD pattern of ZnO prepared by Sol-gel (2$^{nd}$ process) and green synthesis is shown in **Fig 2 (b)**. Nanoparticle formation took place for samples prepared by the Sol-gel process which was evident from the broad and low intensity peaks **[26]**.

Preprints (www.preprints.org) | NOT PEER-REVIEWED | Posted: 26 September 2022 doi:10.20944/preprints202209.0382.v1



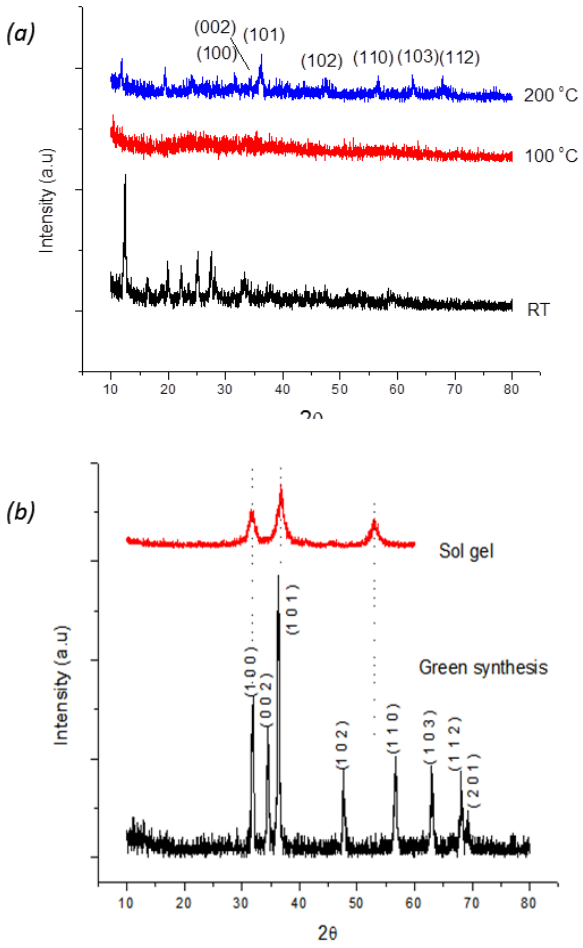


**Fig 1.** (a) XRD of synthesized ZnO nanoparticles at different temperatures (b) XRD of synthesized ZnO nanoparticles by Sol-gel method and green synthesis (reproduced under CC BY License) **[26]**

UV spectra of the samples are shown in **Fig 4 (a)**. The adsorption of light takes place between 200 – 800 nm. The most probable transition takes place form the highest occupied molecular orbital (HOMO) to the lowest unoccupied Molecular orbital (LUMO). An increase in absorption intensity was observed with increase of temperature. Absorption of light occurs in a material due to electronic polarization or excitation. An increase in temperature causes the Zn and O atoms to vibrate along their bond axis (phonons). Higher is the temperature, more will be the vibration. During the vibration, there are instances when the Zn and O atoms are at maximum distance apart. The atoms while vibrating are also creating a vibration in the electron distribution of the existing in the bond. Light being an electromagnetic wave can induce

Preprints (www.preprints.org) | NOT PEER-REVIEWED | Posted: 26 September 2022 doi:10.20944/preprints202209.0382.v1



electronic oscillations in the bonds which may ultimately result into high light absorption. An increase in temperature also causes an increase in number of electrons cutting loose from the valence band and excited to the conduction band which can also result in higher absorption intensity and broadening as observed. The increase in absorption is also due to increase in crystallinity with temperature. However, it should be kept in mind that the frequency of electronic transition is much higher $10^{-15}$ $s^{-1}$ and hence in molecules, the vibrational levels are almost stationary when electronic transitions take place (Franck Condon Principle). In semiconductors however due to formation of excitons with temperature, the scenario is different. A decrease in band gap was observed with increase in temperature as observed from the Tauc plot (**Fig 4b**).

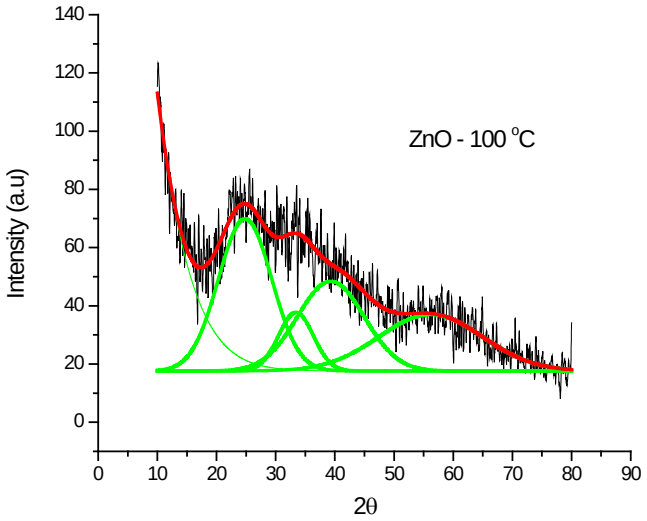


| Area | Center | Width | Height |
|---|---|---|---|
| 588.49662291154 | 24.825688769968 | 8.9866342449739 | 52.250081254654 |
| 147.4963769111 | 33.42061710666 | 5.8473443337668 | 20.126244529867 |
| 434.58432126233 | 39.308885470021 | 11.267268610513 | 30.774816176716 |
| 423.96158213756 | 56.197190932777 | 17.450906315241 | 19.384231090948 |

In degenerately n-doped semiconductor photo excited holes come to the top of the valence band and recombine with an electron with a possible change in k vector. The relaxation of the k-

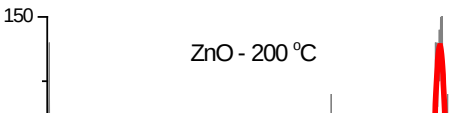

 doi:10.20944/preprints202209.0382.v1



selection rule is caused by crystal imperfection introduced by dopants or by momentum taken up by electron gas.

| Area | Center | Width | Height |
|---|---|---|---|
| 20.737985765733 | 19.38029874361 | 0.264747600084557 | 62.499220434031 |
| 22.734919560847 | 11.781998505335 | 0.27963591068075 | 64.869498572393 |
| 19.384678880344 | 24.154309474021 | 0.53303129492633 | 29.01656270836 |
| 1260.5701171212 | 31.164476569198 | 34.902794424315 | 28.81687414575 |
| 452.40380290352 | 9.0283472740671 | 6.0743121998342 | 59.425001170515 |
| 19.585975045801 | 31.701219246457 | 0.47994840163584 | 32.560473259316 |
| 15.138366348536 | 34.360742420749 | 0.30793495627147 | 39.2247406612516 |
| 61.286155459969 | 36.110709798088 | 0.51534957903619 | 94.885645048795 |
| 183.48724520396 | 64.714415445349 | 11.571246166769 | 12.652193025927 |
| 6.2166304585608 | 40.751594080048 | 0.37785480711192 | 13.127141350972 |

Fig 3: Gaussian fit of XRD of ZnO at 200 $^{o}$C

A shift of the absorption band edge towards higher wavelength (red shift) is observed which corresponds to a change in band gap **[27]**. The sample prepared at RT showed a sharp edge at 275 nm. An increase in temperature to 100 $^{o}$C caused formation of a secondary edge around 330 nm apart from 275nm. A further increase in temperature to 200$^{o}$C caused disappearance of the first edge and the second edge shifted to 350 nm which is in proximity with the values reported earlier.

Preprints (www.preprints.org) | NOT PEER-REVIEWED | Posted: 26 September 2022 doi:10.20944/preprints202209.0382.v1



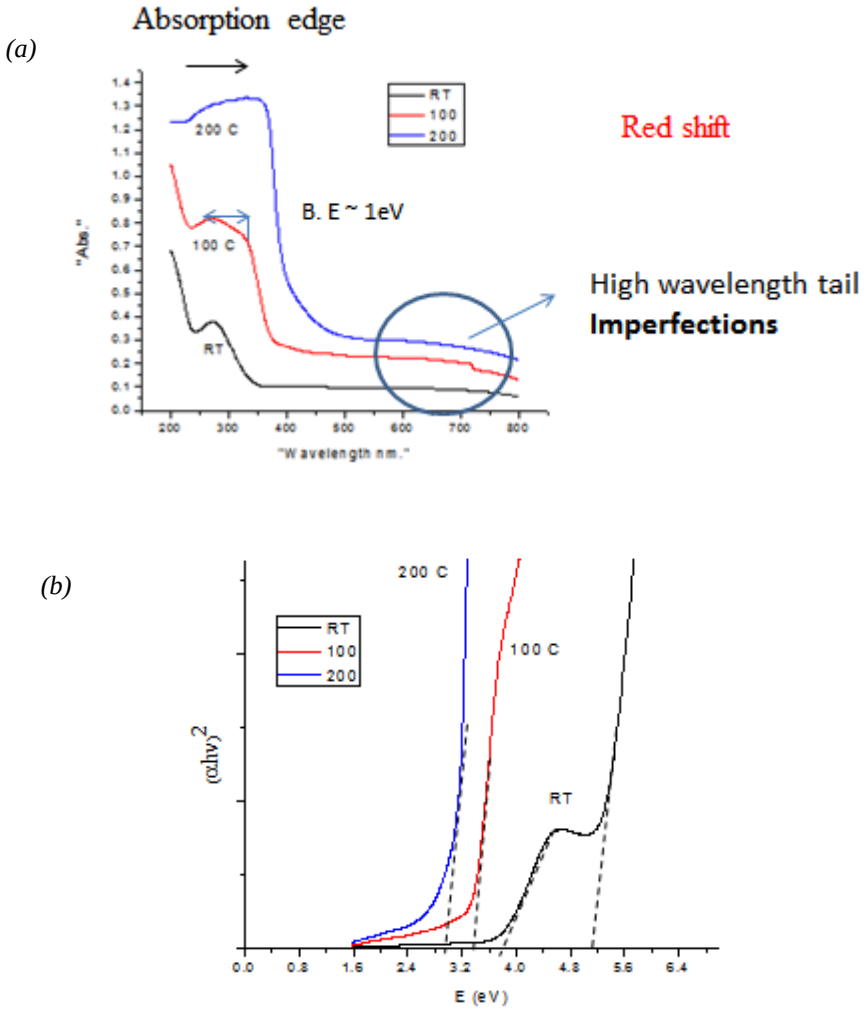


**Fig 4:** (a) UV spectra of synthesized ZnO at different temperatures

(b) Band gap determination from Tauc plot

The first absorption edge at higher wavelength (lower energy) is associated with transfer of electron from filled band to energy bands just below the conduction band called exciton band (**Fig 5**). An exciton is a bound electron hole pair. Since the electron excited is still bound to the hole produced by it by Coulomb field we call it an exciton. It results from transfer of electron from a negative ion which happens to be $O^{-2}$ in this case to the nearest neighbor positive ion ($Zn^{+2}$).

Preprints (www.preprints.org) | NOT PEER-REVIEWED | Posted: 26 September 2022 doi:10.20944/preprints202209.0382.v1



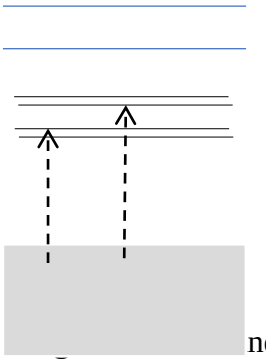


nd formation just below the conduction band

The binding energy of an exciton is $\frac{13.54}{2\epsilon_0^2} \sim$ 1eV for most ionic crystals so the band to band transition should take place 1 eV above the first absorption peak which also was seen experimentally as the difference between the two absorption peaks at 275 nm and 330 nm was almost 1eV. Secondly, as the dielectric constant of a material increases or in other words there is more possibility of polarization in a material, the exciton bands crowd together. For 200 $^{o}$C, the first absorption beak shifts towards higher wavelength (lower energy) due to expansion of lattice leading to lower binding energy of the exciton. The absorption peak also broadens due to increased lattice vibrations at elevated temperatures

The shift in absorption also is related to change in particle size. As the crystallites become larger in size at increased temperature, and there in lowering of energy of first absorption peak, the excitons move in the lattice and transfer the energy to the next negative ion by overlapping of wave functions or dipole coupling.

The initial wave vector k of the exciton is the same as that of the photon which was absorbed to produce it. However, as the exciton propagates through the lattice, it undergoes scattering from lattice imperfections. Lattice imperfections like positive ion vacancy acts like a negative charge and makes it easier to excite electron from the negative ion surrounding it. Hence the outer electrons do not stay in the filled bands but occupy a level above the filled band. The effect of positive ion vacancy is propagated further to the next nearest negative ions which makes them closer to the filled bands. Similarly, a negative ion vacancy acts as a positive charge and attracts electrons which have been created by some means in the conduction band.

Preprints (www.preprints.org) | NOT PEER-REVIEWED | Posted: 26 September 2022 doi:10.20944/preprints202209.0382.v1



This leads to an empty state of the positive ions to lie below the conduction band. An electron in this state can get trapped between the positive ions which are called F-Centers in case of alkali halides. A hole trapped surrounding negative ions due to positive ion vacancy are called V-Centers (**Fig 6**).

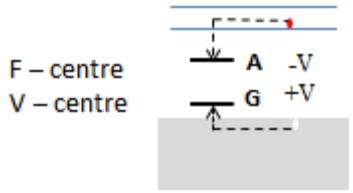


**Fig 6.** Exciton interaction with lattice imperfection forming F and V centers

These new levels also create new absorption band which forms the tail of the first absorption peak. The peak height is proportional to the number of F-Centers per unit volume and hence showed a higher value with increase in temperature indicating formation of more number of lattice defects. The broadening of the peaks at high temperature is due to changed interatomic distance of an excited molecule and Franck Condon principle which states that the vibrational levels being static during an electronic transition (**Fig 7**).

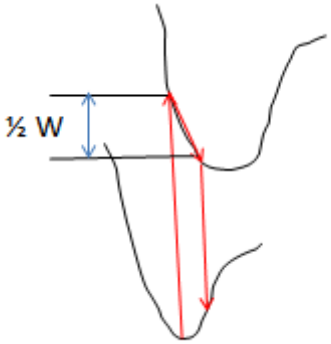


**Fig 7**. Broadening of Absorption peak with temperature

The band gap obtained from Tauc plot $(\alpha h\nu)^{1/n} = A(h\nu - E_g)$ where n = 0.5 for direct transition, showed a variation with change in temperature (Fig 4b). At room temperature two different band gaps were obtained at 3.8 and 5.1 eV respectively. The higher band gap was probably due to the fact that full transformation to ZnO has not yet taken place and a major part of the materials was still in the precursor state as seen in XRD. So we take 3.8 eV as the band gap for this case. On increasing the temperature to 100$^{o}$C a decrease in value to 3.4 eV was observed,

Preprints (www.preprints.org) | NOT PEER-REVIEWED | Posted: 26 September 2022 doi:10.20944/preprints202209.0382.v1



which indicates that the precursor materials have been completely consumed to form ZnO phase. A further rise in temperature to 200 $^{o}$C however caused a decrease in value to 2.9 eV due to formation of defects.

A lattice will expand and contract with rise in temperature which will results in increased oscillations of the atoms around their mean position. The electron lattice interaction also changes with temperature. Impurity potential of donors and acceptors also get affected by rise in temperature. According to Varshini, the band gap is related to temperature as

$$E_g(T) = E_g(0) - \frac{AT^2}{T+B}$$

where A and B are constants **[28]**. The band gap usually shows a slight decrease with rise of temperature.

## 7. Curve fitting of Tauc plot

Curve fitting of the Tauc plots at different temperatures are shown in **Fig 8-10.** The magnitude of the coefficients of E, $E^2$ and $E^3$ which had the major impact on the nature of the curve are given in Table 3. For materials, where there is contribution from two phases the coefficients of $E^2$ and E are close to each other as observed for RT and 100$^{o}$C. For the 200$^{o}$C sample the dominant coefficient was for E indicating formation of only one phase. The effect of different coefficients was analyzed separately and given in **Fig 11-19**.

(a) Sample name: ZnO 100

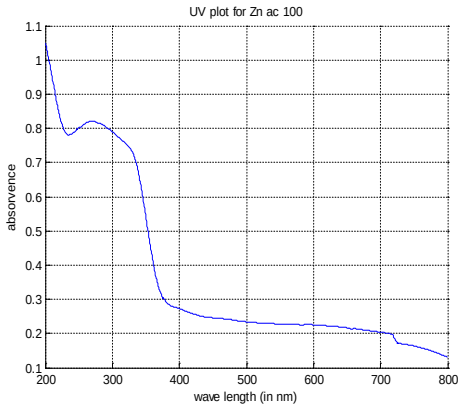


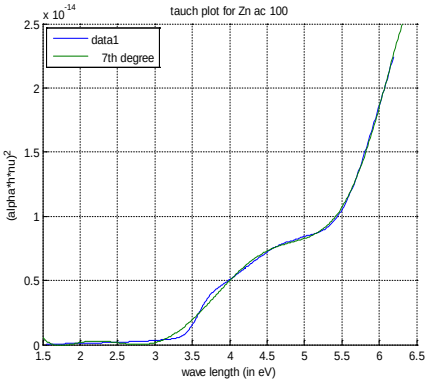

Preprints (www.preprints.org) | NOT PEER-REVIEWED | Posted: 26 September 2022 doi:10.20944/preprints202209.0382.v1



**Fig 8**: Curve Fitting of Tauc plot for ZnO calcined at 100ºC

```
y = p1*x^7 + p2*x^6 + p3*x^5 + p4*x^4 +p5*x^3 + p6*x^2 +p7*x + p8
Coefficients:
p1 = -7.9174e-17; p2 = 2.1288e-15; p3 = -2.3566e-14; p4 = 1.3882e-13; p5 =
-4.6876e-13; p6 = 9.0708e-13; p7 = -9.3235e-13; p8 = 3.9353e-13
```

(b) Sample name: ZnO RT

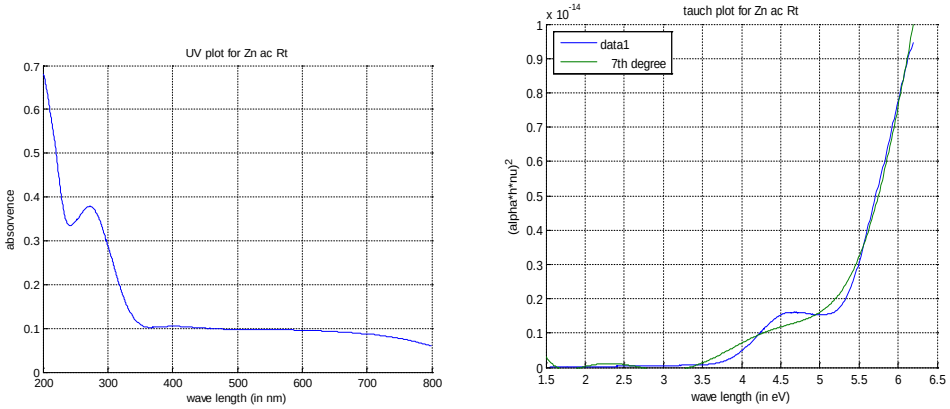


**Fig 9**: Curve Fitting of Tauc plot for ZnO calcined at RT

```
y = p1*x^7 + p2*x^6 + p3*x^5 + p4*x^4 + p5*x^3 + p6*x^2 +p7*x + p8

Coefficients:
p1 = -2.8984e-17; p2 = 7.8261e-16; p3 = -8.7252e-15; p4 = 5.1989e-14; p5 = -
1.7845e-13; p6 = 3.5246e-13; p7 = -3.7077e-13; p8 = 1.6037e-13
```

(c) Sample name: ZnO 200

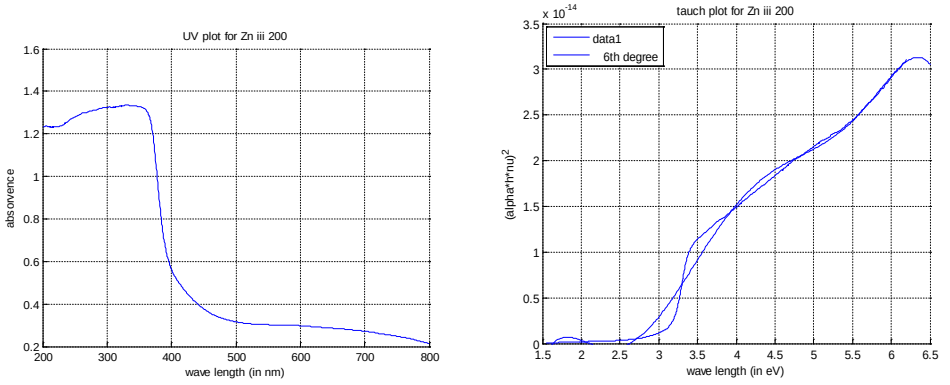


**Fig 10**: Curve Fitting of Tauc plot for ZnO calcined at 200ºC

```
y = p1*x^6 + p2*x^5 + p3*x^4 + p4*x^3 + p5*x^2 + p6*x + p7
Coefficients:
```

Preprints (www.preprints.org) | NOT PEER-REVIEWED | Posted: 26 September 2022 doi:10.20944/preprints202209.0382.v1



```
p1 = -1.926e-16; p2 = 4.6831e-15; p3 = -4.5479e-14; p4 = 2.2393e-13; p5 = -
5.8364e-13;p6 = 7.6213e-13; p7 = -3.9066e-13
```

Table 3 : The variation of coefficients E, $E^2$ and $E^3$ in the scale of $10^{-13}$

| **Temp** | **($E^3$)** | **($E^2$)** | **(E)** |
|---|---|---|---|
| RT | 1.8 | 3.5 | 3.7 |
| 100 | 4.7 | 9.0 | 9.2 |
| 200 | 2.2 | 5.8 | 7.6 |

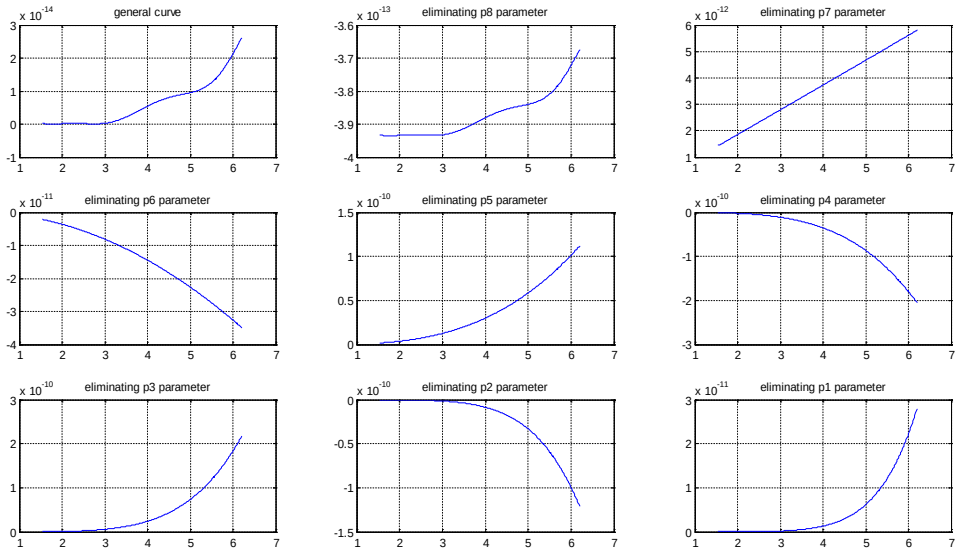


**Fig 11** : Plots by eliminating parameters from p8 through p1:

Preprints (www.preprints.org) | NOT PEER-REVIEWED | Posted: 26 September 2022 doi:10.20944/preprints202209.0382.v1



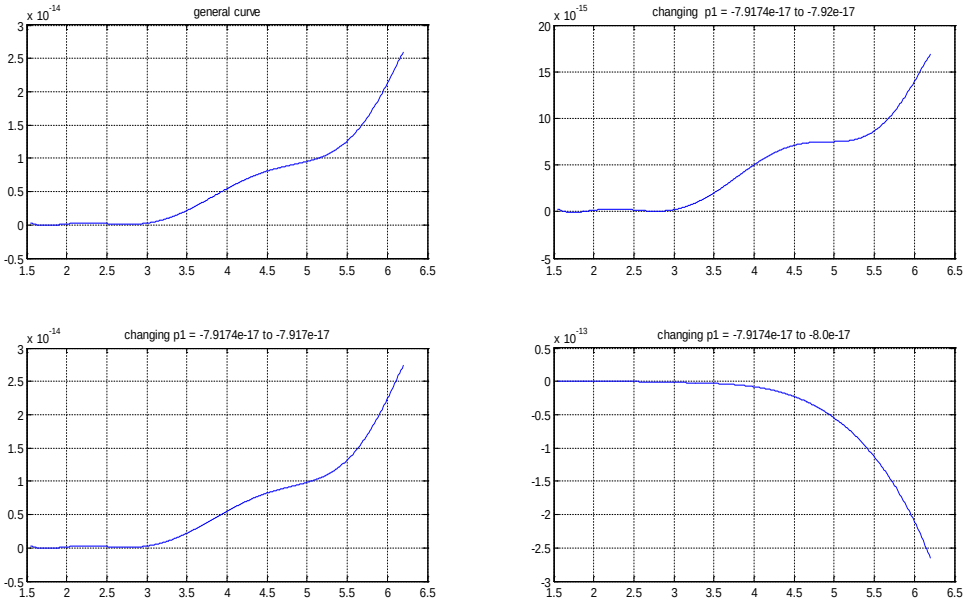


Fig 12 Plots by replacing corresponding parameter rounding off to upper and lower near values (p1):

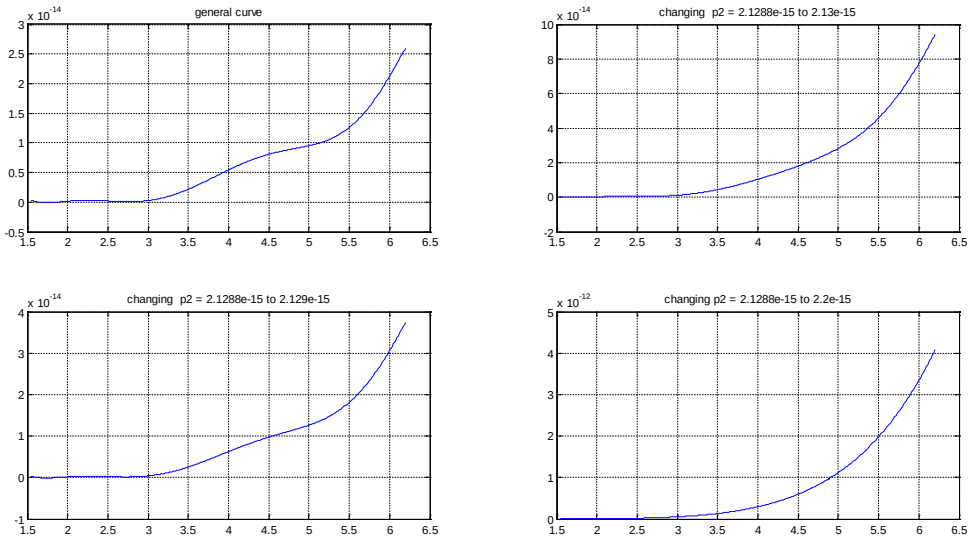


Fig 13: Plots by replacing corresponding parameter rounding off to upper and lower near values (p2):

Preprints (www.preprints.org) | NOT PEER-REVIEWED | Posted: 26 September 2022 doi:10.20944/preprints202209.0382.v1



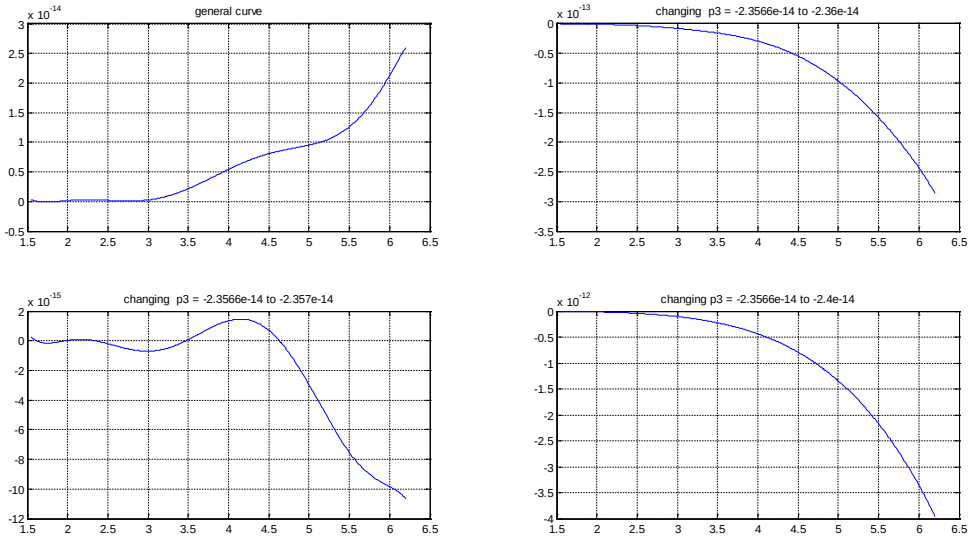


Fig 14 : Plots by replacing corresponding parameter rounding off to upper and lower near values(p3):

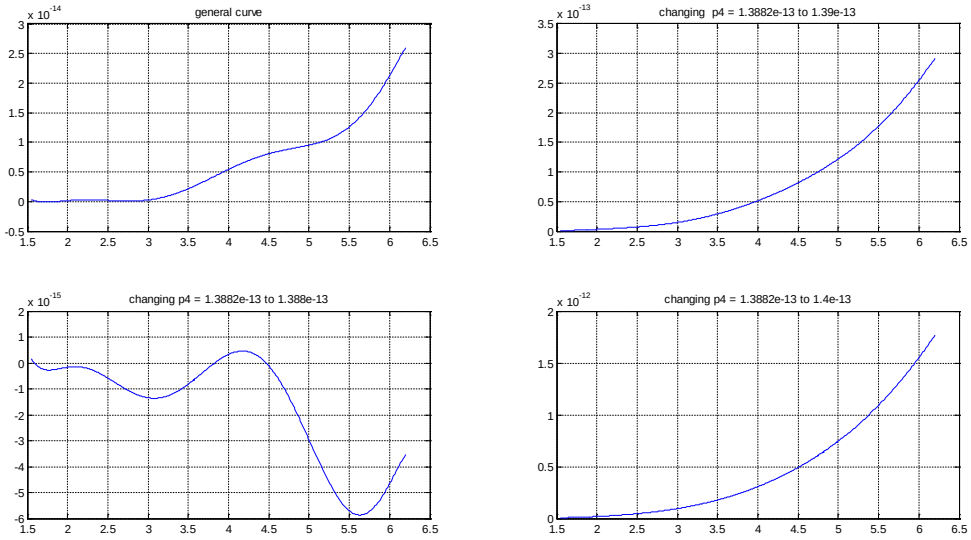


Fig 15: Plots by replacing corresponding parameter rounding off to upper and lower near values(p4):

Preprints (www.preprints.org) | NOT PEER-REVIEWED | Posted: 26 September 2022 doi:10.20944/preprints202209.0382.v1



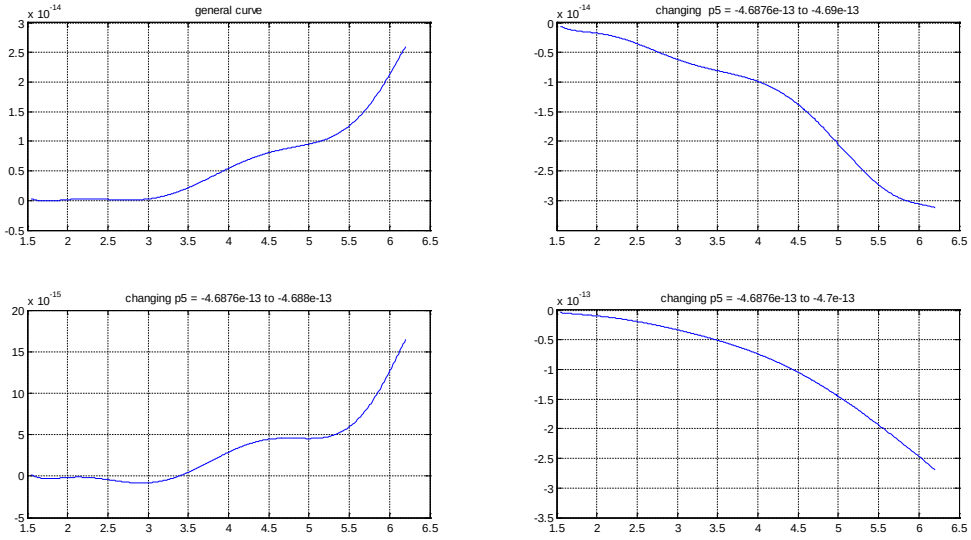


Fig 16: Plots by replacing corresponding parameter rounding off to upper and lower near values(p5):

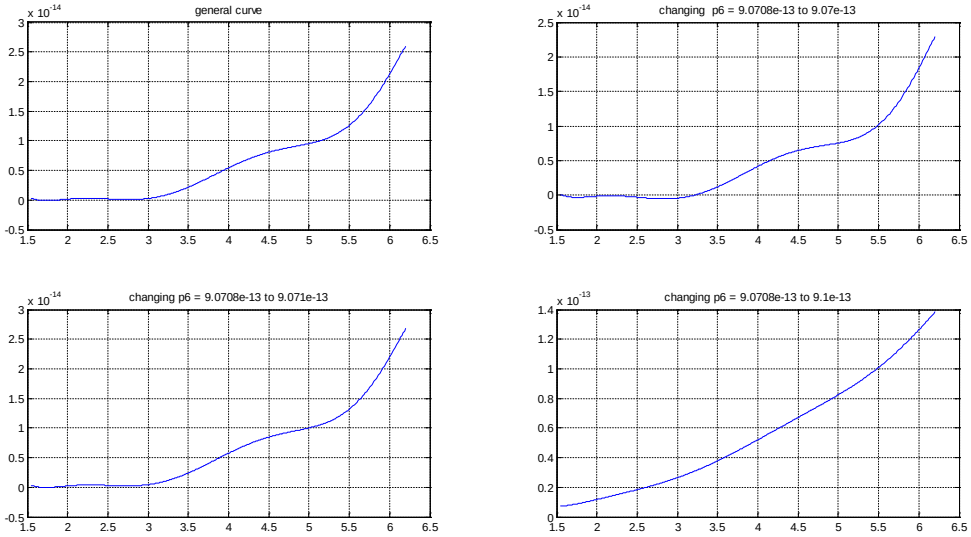


Fig 17 : Plots by replacing corresponding parameter rounding off to upper and lower near values(p6):

Preprints (www.preprints.org) | NOT PEER-REVIEWED | Posted: 26 September 2022 doi:10.20944/preprints202209.0382.v1



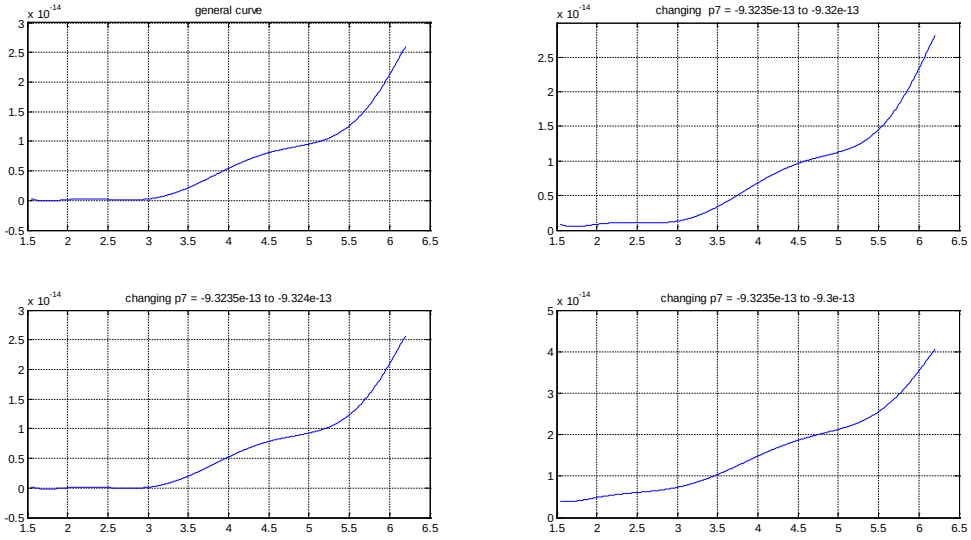


Fig18: Plots by replacing corresponding parameter rounding off to upper and lower near values(p7):

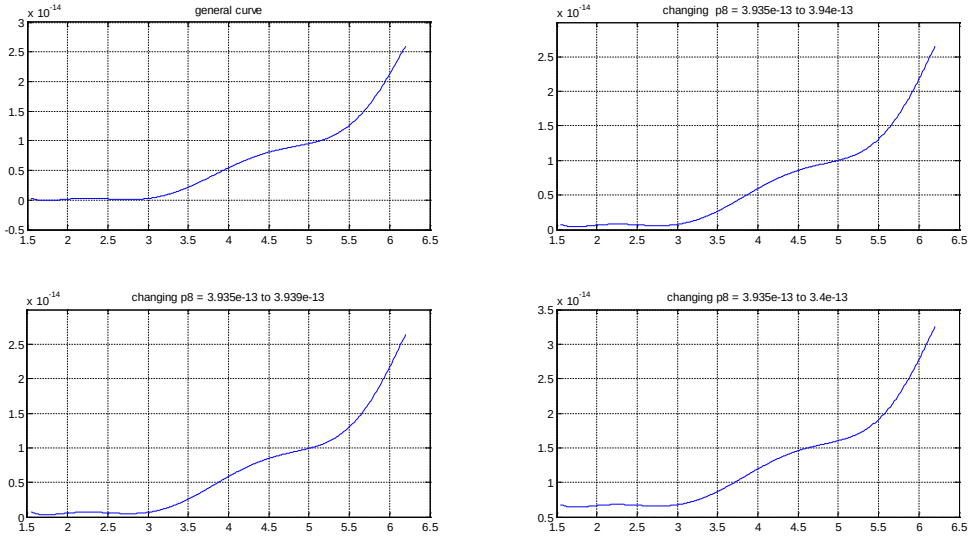


Fig 19 Plots by replacing corresponding parameter rounding off to upper and lower near values (p8):

## 8. Conclusions

ZnO was prepared by Sol gel method at different calcination temperatures. Nucleation of ZnO crystallites at 100 $^{o}$C and their growth with rise in temperature was observed. Exciton bands and lattice imperfections affected the absorption spectra. The decrease in band gap with

temperature was due to the formation of defect energy levels. Phonon assisted non-radiative transitions caused broadening of the peaks. The possibility of tuning the band gap of ZnO by changing the temperature was explored. Simulation studies showed transition to single phase with rise in temperature.

Acknowledgements
The authors would like to thank the UG students of the Dept. of Nanoscience and Technology for their cooperation.

Reference

1. H. Beitollahi, S. Tajik, F. G. Nejad, M. Safaei, ***J. Mater. Chem. B*** (2020) **8,** 5826-5844.
2. R. S. Rai, V. Bajpai, Adv Nano Res, 11 (1) (2021) 37-54.
3. Liu, S.Y.; Wang, R.C.; Ma, C.X.; Yang, D.H.; Li, D.X.; Lewandowski, Z. Improvement of Electrochemical Performance via Enhanced Reactive Oxygen Species Adsorption at ZnO–NiO@rGO Carbon Felt Cathodes in Photosynthetic Algal Microbial Fuel Cells. Chem. Eng. J. 2020, 391, 123627.
4. Murali, S.; Dammala, P.K.; Rani, B.; Santhosh, R.; Jadhao, C.; Sahu, N.K. Polyol Mediated Synthesis of Anisotropic ZnO Nanomaterials and Composite with rGO: Application towards Hybrid Supercapacitor. J. Alloys Compd. 2020, 844, 156149.
5. Chen, X.Y.; Wang, X.Z.; Liu, F.J.; Song, X.J.; Cui, H.Z. Fabrication of NiO–ZnO-modified g-C3N4 Hierarchical Composites for High-performance Supercapacitors. Vacuum 2020, 178, 109453.
6. Ouyang, Y.; Xia, X.F.; Ye, H.T.; Wang, L.; Jiao, X.Y.; Lei, W.; Hao, Q.L. Three-dimensional Hierarchical Structure ZnO@C@NiO on Carbon Cloth for Asymmetric Supercapacitor with Enhanced Cycle Stability. ACS Appl. Mater. Interfaces 2018, 10, 3549–3561.
7. Angelin, M.D.; Rajkumar, S.; Merlin, J.P.; Xavier, A.R.; Franklin, M.; Ravichandran, A.T. Electrochemical Investigation of Zr-doped ZnO Nanostructured Electrode Material for High-performance Supercapacitor. Ionics 2020, 26, 5757–5772.

 doi:10.20944/preprints202209.0382.v1




8. Naeem, F.; Naeem, S.; Zhao, Z.; Shu, G.Q.; Zhang, J.; Mei, Y.F.; Huang, G.S. Atomic Layer Deposition Synthesized ZnO Nanomembranes: A Facile Route towards Stable Supercapacitor Electrode for High Capacitance. J. Power Sources 2020, 451, 227740.
9. Miah, M.; Mondal, T.K.; Ghosh, A.; Saha, S.K. Study of Highly Porous ZnO Nanospheres Embedded Reduced Graphene Oxide for High Performance Supercapacitor Application. Electrochim. Acta 2020, 354, 136675.
10. Liu, J.; Xu, T.; Sun, X.W.; Bai, J.; Li, C.P. Preparation of Stable Composite Porous Nanofibers Carried SnOx-ZnO as a Flexible Supercapacitor Material with Excellent Electrochemical and Cycling Performance. J. Alloys Compd. 2019, 807, 151652.
11. Kumar, R.; Youssry, S.M.; Abdel-Galeil, M.M.; Matsuda, A. One-pot Synthesis of Reduced Graphene Oxide Nanosheets Anchored ZnO Nanoparticles via Microwave Approach for Electrochemical Performance as Supercapacitor Electrode. J. Mater. Sci.-Mater. Electron. 2020, 31, 15456–15465.
12. Chaudhary, S.; James, L.S.; Kumar, A.B.V.K.; Ramana, C.V.V.; Mishra, D.K.; Thomas, S.; Kim, D. Reduced Graphene Oxide/ZnO Nanorods Nanocomposite: Structural, Electrical and Electrochemical Properties. J. Inorg. Organomet. Polym. Mater. 2019, 29, 2282–2290.
13. Wang, W.; Jiao, S.S.; Cao, J.Y.; Naguib, H.E. Zinc Oxide/carbon Nanotube Nanocomposite for High-performance Flexible Supercapacitor with Sensing Ability. Electrochim. Acta 2020, 350, 136353.
14. Arunpandiyan, S.; Bharathi, S.; Pandikumar, A.; Arasi, S.E.; Arivarasan, A. Structural Analysis and Redox Additive Electrolyte Based Supercapacitor Performance of ZnO/CeO2 Nanocomposite. Mat. Sci. Semicon. Proc. 2020, 106, 104765.
15. Shaheen, I.; Ahmad, K.S.; Zequine, C.; Gupta, R.K.; Thomas, A.G.; Malik, M.A. Green Synthesis of ZnO-Co3O4 Nanocomposite Using Facile Foliar Fuel and Investigation of Its Electrochemical Behaviour for Supercapacitors. New J. Chem. 2020, 44, 18281–18292.
16. Zhou, H.Y.; Fu, W.B.; Muhammad, M.; Xie, M.Z.; Xie, E.Q.; Han, W.H. Self-assembled Microspheres Composed of Porous ZnO/CoO Nanosheets for Aqueous Hybrid Supercapacitors. J. Phys. D Appl. Phys. 2019, 52, 505501.

17. Chakraborty, S.; Raj, M.A.; Mary, N.L. Biocompatible Supercapacitor Electrodes Using Green Synthesised ZnO/Polymer Nanocomposites for Efficient Energy Storage Applications. J. Energy Storage 2020, 28, 101275.
18. Simon, R.; Chakraborty, S.; Konikkara, N.; Mary, N.L. Functionalized Polystyrene Maleic Anhydride Copolymer/ZnO Nanocomposites for Enhanced Electrochemical Performance. J. Appl. Polym. Sci. 2020, 137, 48945.
19. Chebrolu, V.T.; Balakrishnan, B.; Cho, I.; Bak, J.S.; Kim, H.J. A Unique Core-shell Structured ZnO/NiO Heterojunction to Improve the Performance of Supercapacitors Produced Using a Chemical Bath Deposition Approach. Dalton Trans. 2020, 49, 14432–14444.
20. Di, S.; Gong, L.G.; Zhou, B.B. Precipitated Synthesis of $Al_2O_3$-ZnO Nanorod for High-Performance Symmetrical Supercapacitors. Mater. Chemi. Phys. 2020, 253, 123289.
21. Liu, X.J.; Liu, H.; Sun, X.Z. Aligned ZnO nanorod@Ni–Co Layered Double Hydroxide Composite Nanosheet Arrays with a Core–shell Structure as High-performance Supercapacitor Electrode Materials. CrystEngComm 2020, 22, 1593–1601.
22. G. Kaur, A. Mitra, K.L. Yadav. Progress in Natural Science: Materials International 25 (2015) 12–21
23. M. Akhtar, H. Alhadlaq, A. Alshamsan, A. *et al. Sci Rep* **5,** 13876 (2015).
24. M.M. Khan, S. Kumar, M.N. Khan, M. Ahamed, A. S. Al Dwayyan. *Journal of luminescence, 155* (2014) 275-281.
25. Octave Online · Cloud IDE compatible with MATLAB (octave-online.net)\
26. P. Mahapatra, S. Kumari, Simran, S. Sharma, K. Gaurav, N. Kumari, P. Kommu, P. Prabhakar and A.S. Bhattacharyya *Mat. Sci. Res. India* 13 (1) (2016) 07-13.
27. O. A. Novodvorsky, Novodvorsky, O.A., L. S. Gorbatenko, V. Y. Panchenko, et. al *Semiconductors* 43 (4), 419 (2009)
28. Y.P. Varshni, *Physica*, 34 1967, 149-154.